Aggregates from Perylene Bisimide Oligopeptides as a Test Case for Giant Vibrational Circular Dichroism

Marty, Roman ; Frauenrath, Holger ; Helbing, Jan

Abstract: Vibrational circular dichroism (VCD) spectroscopy has become an excellent tool to study biological nanostructures and biomimetic materials in their functional environment and is thus complementary to otherwise employed diffraction, imaging, and spectroscopy methods. However, it is still difficult to relate the observed exceptionally large VCD signals to specific structural elements. Here, we systematically studied the VCD signatures of structurally well-defined and thoroughly characterized nanofibrils from oligopeptide-substituted perylene bisimides that comprise single parallel -sheets. These nanofibrils show a giant VCD signal in the absence of -sheet stacking and a negative VCD couplet despite their right-handed helicity. The giant VCD signal was very sensitive to subtle changes in the molecular structure as well as 13 C-labeling, which caused a strong disruption of the exciton system as confirmed by two-dimensional infrared spectroscopy. Simulations based on the commonly applied transition dipole coupling model qualitatively reproduced the IR spectra but failed to account for the observed giant VCD or the strong isotope effect. Because our model system and isotope labeling imposes stringent structural constraints of the observed spectroscopic features, our results challenge current assumptions regarding the structural parameters determining VCD sign and intensity. The investigated system may, hence, serve as a benchmark for more sophisticated models with better predictive power for the investigation of protein aggregates in biomedical context or novel oligopeptide-based nanomaterials.

DOI: https://doi.org/10.1021/jp506837c

Single β-Sheets from Perylene Bisimide Oligopeptides – A Test Case for Giant Vibrational Circular Dichroism

*Roman Marty[1], Holger Frauenrath[1], and Jan Helbing[2]**

[1] Ecole Polytechnique Fédérale de Lausanne (EPFL), Switzerland
Institute of Materials
Laboratory of Macromolecular and Organic Materials

EPFL – STI – IMX – LMOM, MXG 037, Station 12
1015 Lausanne, Switzerland

[2] University of Zurich, Switzerland
Department of Chemistry

Winterthurerstrasse 190
8057 Zurich, Switzerland

jan.helbing@chem.uzh.ch

Abstract

Vibrational circular dichroism (VCD) spectroscopy is an excellent tool to study oligopeptide self-assembly in solution that is complementary to the diffraction, imaging, and spectroscopy methods typically used for the investigation of biological nanostructures and biomimetic materials in their functional environment. However, it is still difficult to relate the observed exceptionally large VCD signals to specific structural properties. Here, we systematically study the VCD signatures of highly reproducible, well-characterized nanofibrils from oligopeptide-substituted perylene bisimides. These nanofibrils comprise single parallel β-sheets that show a giant VCD signal in the absence of β-sheet stacking, and a negative VCD couplet despite their right-handed helicity. The giant VCD signal was observed only for a specific length of the oligopeptide chains and almost completely disappeared upon ^{13}C isotope labelling, which caused a strong disruption of the exciton system, as confirmed by two-dimensional infrared spectroscopy. Simulations based on a transition dipole coupling model qualitatively reproduced the IR spectra but failed to account for the observed giant VCD or the strong isotope effect. Since our model system and isotope labeling imposes stringent structural constraints on the observed spectroscopic features, our results challenge current assumptions regarding the structural parameters determining VCD sign and intensity and may, hence, serve as a benchmark for more sophisticated models with better predictive power for novel chiral nanomaterials.

Keywords

Vibrational Circular Dichroism, 2D Infrared Spectroscopy, Organic Nanowires, Supramolecular Self-Assembly, Perylene Bisimides, Oligopeptide β-sheet, Coupled Dipole Simulations

Introduction

The investigation of complex biological nanostructures and biomimietic materials in their functional environment will require additional structure analysis tools beyond diffraction and imaging methods or multidimensional NMR spectroscopy. Vibrational circular dichroism (VCD) spectroscopy offers a unique probe of oligopeptide self-assembly into fibrillar nanostructures in solution that is complementary to imaging methods such as AFM or SEM. Since the first report in 2007,[1] the exceptionally large vibrational circular dichroism (VCD) signal of the amide I band of amyloid fibrils,[2-4] peptidomimetics in β-sheet conformation,[5-8] as well as in helical polymers of isocyanopeptides[9,10] and supramolecular assemblies[11] has attracted considerable attention. While it was immediately clear that the enhanced VCD intensity must be the result of supramolecular chiral order, it remains challenging to correlate the large variations of signal shape, size or sign to structural parameters. Amyloid fibrils of human insulin, for example, exhibit an intense negative VCD couplet for the amide I absorption (a so-called 'normal' couplet with a negative-positive transition with increasing wavenumber) which is associated to fibrils with explicit left-handed helical surface morphology.[2] By contrast, incubation at lower pH yields flat tape-like fibrils with no obvious helical surface morphology according to electron microscopy imaging. Nevertheless, these tapes showed intense VCD spectra that were mirror images of the 'normal' ones (reversed couplet). In fact, no example of oligopetide aggregates has been reported in the literature to date in which a right-handed helical surface morphology could be clearly correlated with a reverse Cotton effect in VCD.

In order to better understand the coupling mechanisms that may be at the origin of the enhanced VCD signals, isotope labeling has been used to decouple single or multiple amino acids from the main amide I mode, allowing to investigate the site-specific local peptide conformation and dynamics.[6,8,12-14] In a complementary approach, different contributions to the amide I band of peptides and proteins have been disentangled in two-dimensional IR spectroscopy (2D-IR) investigations,[15-17] which were recently extended to study amyloid fibrils.[18-20] In order to aid the interpretation of the spectral patterns, methods initially developed for the simulation of single oligopeptides have been applied to aggregate models.[19,21] Keiderling *et al.* have recently performed DFT computations on short oligo(L-alanine) β-strands as well as single stacked β-sheets, and developed a qualitative set of spectral signatures suitable for the

discrimination of specific structural features of β-sheet-based aggregates.[22-24] Schweitzer-Stenner *et al.* had previously investigated similar systems using the simpler transition dipole coupling formalism.[25,26] Although such simulations did not fully reproduce the remarkably large VCD signals observed experimentally for oligopeptide fibrils, they suggest that VCD enhancement is primarily due to β-sheet stacking.

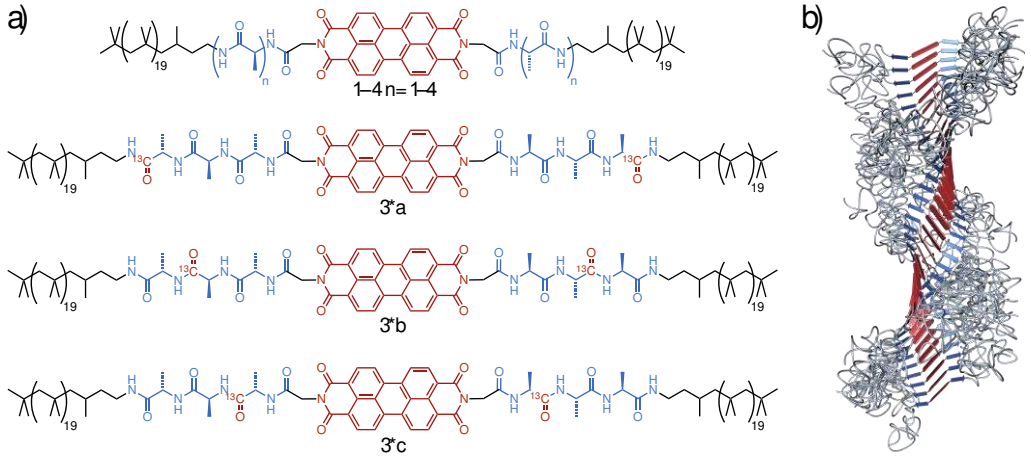

Figure 1. *a)* Oligopeptide-substituted perylene bisimides with $n = 1–4$ unlabeled L-alanine units (**1**–**4**) or ^{13}C-labeled oligopeptides (**3*a**–**c**). *b)* Schematic illustration of a one-dimensional aggregate with a single stack of the π-conjugated molecules at their core (red), flanked by two helically intertwined but structurally isolated parallel β-sheets (blue arrows represent the individual β-strands and mark the direction of the *C*-termini).

Inspired by the hierarchical organization of β-sheet-forming oligopeptides into amyloid fibrils,[27,28] we previously reported an example well-defined nanofibrils formed from a single stack of the oligopeptide-polymer-substituted perylene bisimides **1**–**4**.[29-31] According to our detailed structural characterization of these systems, they may serve as a model system for helically twisted, single β-sheets. In the present work, we therefore investigated nanofibrils from **1**–**4** with $n = 1–4$ L-alanine residues per side group, as well as the ^{13}C-labeled derivatives **3*a**–**c** with tri(L-alanine) substituents and ^{13}C-labeled carbonyl groups in the outer, middle, and innermost L-alanine residues (Figure 1), respectively, by means of VCD and 2D-IR spectroscopy, complemented with simulations based on the coupled dipole model. We observed that the nanofibrils of **3** exhibited a giant VCD signal that was highly sensitive to isoptope labeling and, due to the nature of our model system, cannot have its origin in β-sheet stacking. Moreover, we provide the first example of an oligopeptide aggregate with an explicitly right-handed supramolecular helicity that gives rise to a negative ('normal') VCD couplet for the

amide I absorption, suggesting that the sign of the VCD couplet may not be a unique indicator of the helix handedness. Since our model system and isotope labeling imposes stringent structural constraints of the observed spectroscopic features, our results may hence serve as an incentive to devlop more sophisticated models that will be required to establish VCD spectroscopy as an authorative method to derive reliable structural information from peptide-based nanostructures and materials in their functional environement.

Results and Discussion

Synthesis and AFM imaging. For our investigations, we prepared the oligopeptide-polymer-functionalized perylene bisimides **1**–**4** and **3*a**–**c** by solution-phase peptide coupling and deprotection reactions starting from poly(isobutylene) amine, isotope-labeled and regular L-alanine derivatives, as well as perylene bisimide building blocks, similar to previously published strategies (Supplementary Schemes S1–S2).[29,31,32] Consistent with our previous in-depth investigation of such nanofibrils,[30] atomic force microscopy (AFM) imaging of samples on mica substrates from thermally annealed 1,1,2,2-tetrachloroethane (TCE) solutions of **1**–**4** and **3*a**–**c** revealed the presence of well-defined nanofibrils with lengths of several micrometers (Figure 2a, Supplementary Figure S1).[31] For the scope of the subsequent spectroscopic investigations, it is important to note that the AFM images revealed regular height corrugations with a periodicity of 82 ± 8 nm and height maxima ("bumps") of 3.7 ± 0.2 nm as well as minima ("grooves") of 3.0 ± 0.1 nm (Figure 2a–c, Supplementary Figures S2–S3). Moreover, the phase images showed the height maxima to exhibit "diagonal" features that exhibited characteristic height corrugations themselves (Figure 2c, Supplementary Figure S2). These observations provided clear evidence that nanofibrils of **3** exhibited a right-handed supramolecular helicity, supposedly in the form of helically curled tapes (Figure 1b). In all cases, AFM phase images taken at higher magnification proved that the occasionally observed broader features were not fibrillar bundles obtained by β-sheet stacking, but simply laterally aligned individual nanofibrils with a defined width of 7–8 nm (Figure 2b, Supplementary Figures S1 and S4). Accordingly, assuming an intermolecular distance of 4.6 Å within the fibrils,[30] the available volume per molecule amounts to about 8700 $Å^3$ in the "groove" regions

of the nanofibrils. Since the van der Waals volumes of **1**–**4** and **3*a**–**c** is on the order of 5800 Å^3, one can strictly conclude that all aggregates are formed from a single helical stack of the constituting molecules and do not exhibit β-sheet stacking.

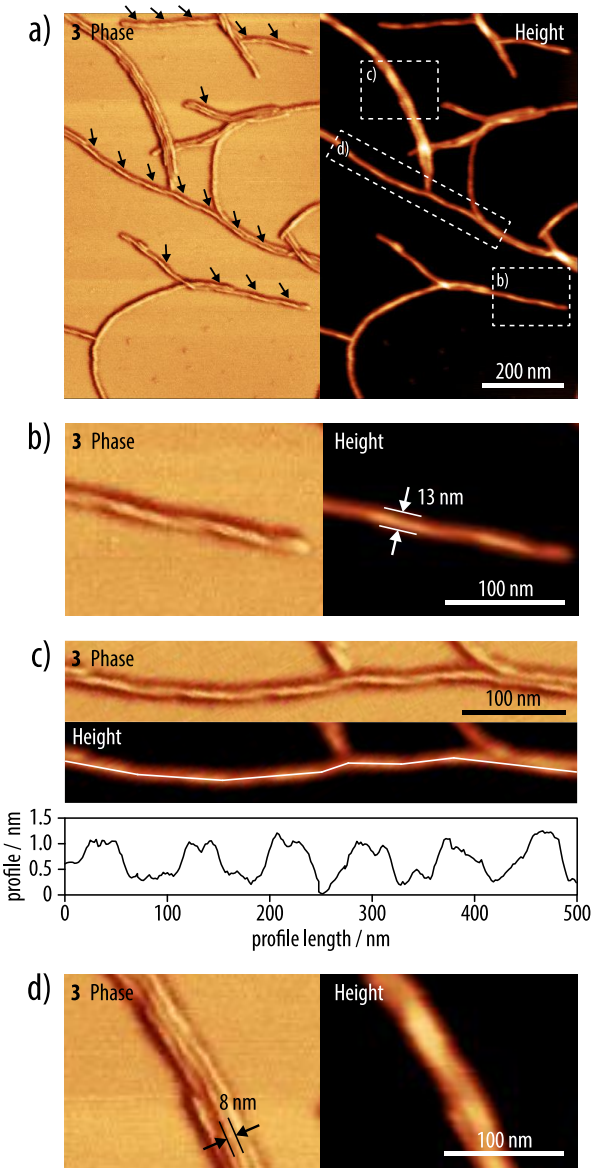

Figure 2. *a–b)* AFM phase and height images of compound **3** on a mica substrate proved the presence of several micrometers long right-handed helically twisted nanofibrils exhibiting periodic corrugations along the fibril axis (indicated by the black arrows in the phase image). *c)* A height profile analysis along a nanofibril revealed that the height maxima exhibited a characteristic height profile themselves. *d)* The occasionally observed broader features were constituted from laterally aligned individual nanofibrils with a defined width of 7–8 nm.

Linear Spectroscopy in Solution. Consistent with the formation of nanofibrils as revealed by AFM imaging, the solution-phase UV/vis spectra of **3** and the corresponding ^{13}C-labeled compounds **3*a**–**c** showed a strongly blue-shifted peak absorption along with additional red-

shifted components (compared to molecularly dissolved perylene bisimides) due to excitonic coupling of the π–π stacked perylene bisimides (Figure 3a, top).[30] More importantly, all solutions showed electronic circular dichroism (ECD) spectra with a positive Cotton effect for the highest wavelength absorption at 602 nm, a zero-transition at 468 nm, and a negative signal at 438 nm (Figure 3a, bottom). This finding implies that the stacked perylene bisimides are in a *P*-helical (right-handed helical) environment,[33-35] confirming independently the right-handed helicity of the aggregates observed in AFM imaging.

Whereas the UV/vis and CD spectra of **3** and its isotope-labled siblings **3*a**–**c** were virtually identical, drastic differences were observed in their vibrational spectra. In the amide I region of the FTIR spectrum (Figure 3b, top), a sharp band at 1631 cm^{-1} in the IR spectrum of **3** as well as the absence of the secondary amide I component at 1695 cm^{-1} were consistent with the formation parallel β-sheet-like aggregates. In the case of **3*a** with the ^{13}C-labeled carbonyl on the outermost L-alanine in each oligopeptide strand, the main amide I band exhibited a marginal blue shift to 1633 cm^{-1} as well as a slightly reduced oscillator strength. The amide I contribution of the ^{13}C-labeled carbonyls produced a new band at 1606 cm^{-1} due to the larger reduced mass for $^{13}C{=}O$ as compared to $^{12}C{=}O$. For **3*b** and **3*c** with the ^{13}C-labels on the middle or the innermost L-alanines, respectively, the main amide I band split into two bands at 1653 and 1639 cm^{-1}, indicating a disruption of the excitonic system of the regular (^{12}C) amide I components. At the same time, the amide I contribution of the $^{13}C{=}O$ groups experienced a further red shift to 1603 and 1601 cm^{-1} for **3*b** and **3*c**, respectively. All derivatives exhibited additional absorptions at 1701, 1666, and 1595 cm^{-1} associated with carbonyl and C=C stretch vibrations of the perylene bisimide core.[36] A substraction of the simulated perylene bisimide bands from the regular FTIR spectra illustrated the above discussed features even more clearly (Figure 3b, middle).

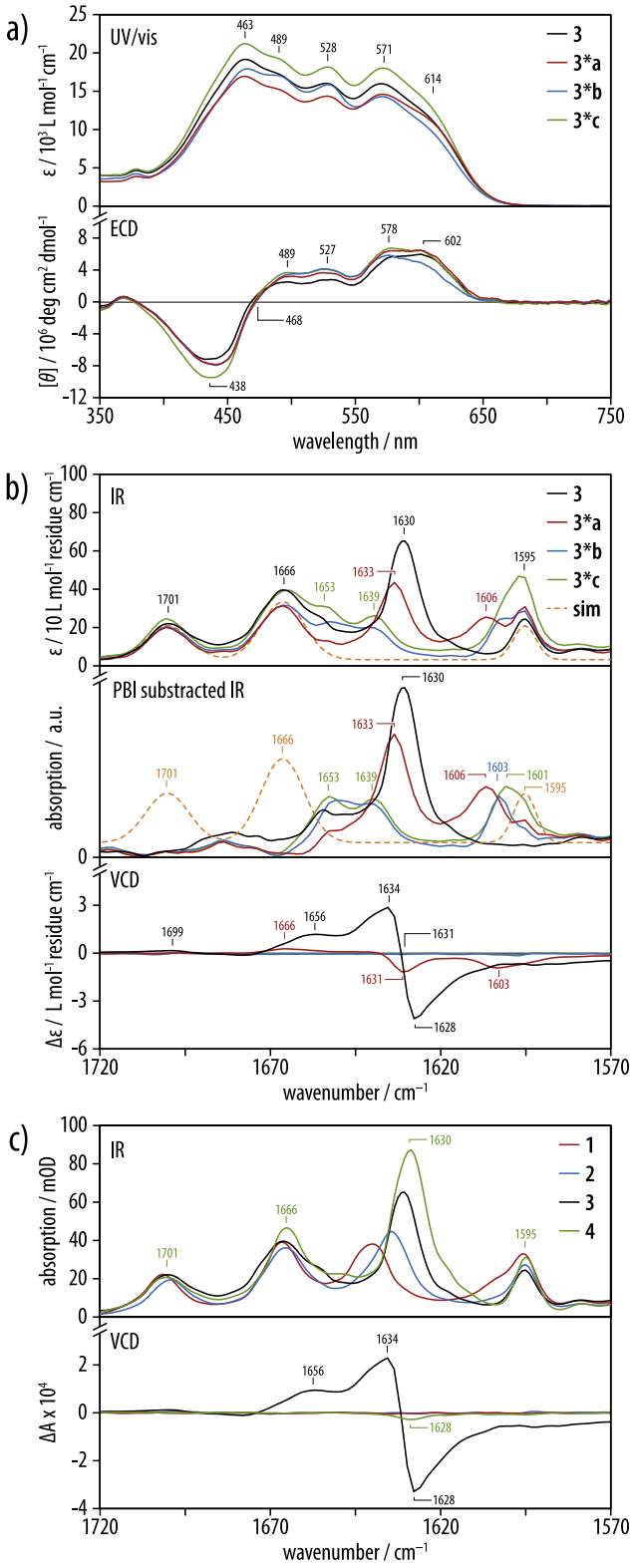

Figure 3. *a)* The solution-phase UV/vis (top) and ECD spectra (bottom) of **3**, and **3*a–c** in TCE ($1 \cdot 10^{-4}$ mol/L) were almost identical, which proved that ^{13}C-labeling of the L-alanine carbonyl groups had negligible impact on the internal order of the nanofibrils. *b)* By contrast, the solution-phase FTIR spectra before (top) and after substraction of the simulated perylene bisimide bands (middle, orange dashed lines) as well as the VCD spectra (bottom) in TCE ($1 \cdot 10^{-3}$ mol/L) of the ^{13}C-labeled compounds **3*a–c** revealed significant differences compared to the unlabeled derivative **3** that was the only compound to exhibit a giant VCD with a $\Delta\varepsilon/\varepsilon$ ratio of $4.4 \cdot 10^{-3}$. *c)* Solution-phase IR (top) and VCD spectra (bottom) in TCE ($1 \cdot 10^{-3}$ mol/L) of compounds **1–4** with a variable number of n = 1–4 unlabeled L-alanine units per side chain.

Remarkably, VCD spectroscopy of aggregates of the unlabeled compound **3** produced a giant negative VCD couplet for the amide I band, with main bands at 1628 and 1634 cm^{-1} and a $\Delta\varepsilon/\varepsilon$ ratio of $4.4 \cdot 10^{-3}$ (Figure 3b, bottom). The latter value is about two orders of magnitude larger than typically observed for single β-sheets and comparable to values reported for mature amyloid fibrils.[1-11] Moreover, it is worth noting that we observed a negative ('normal') VCD couplet for the explicitly right-handed helical aggregates according to AFM imaging. Besides the main VCD bands, weaker signals at 1656 and 1699 cm^{-1} may indicate that the perylene bisimide C=O stretch vibrations were partially coupled to the excitonic system of the amide I band. Drastic changes in the VCD spectra were observed upon isotope-labeling (Figure 3b, bottom). In the case of **3*a**, the signal intensity was significantly reduced, and negative VCD signals at 1631 and 1603 cm^{-1} were observed for both the main amide I mode as well as the isotope-shifted absorption band. This may be expected in case of a partial redistribution of the oscillator strength in favor of the isotope-shifted band. Again, a small positive contribution at 1666 cm^{-1} indicated a partial coupling of the perylene bisimide C=O stretch vibrations to the amide I band. By contrast, positioning the isotope labels closer to the perylene bisimide cores in **3*b** and **3*c** resulted in an unexpected, almost complete disappearance of the VCD signal. In order to checked if this isotope effect can be explained by the effective number of coupled neighboring carbonyls we investigated aggregates of **1–4** with oligo(L-alanine) β-strands of different length and observed a monotonous shift of the amide I absorption towards lower frequencies, consistent with a continuous growth of the exciton system (Figure 3c, top). Interestingly, however, while **1** and **2** showed no VCD at all and **3** produced the giant VCD signal described above, the further elongation of the β-strand in **4** produced only a comparably weak and negative band at 1628 cm^{-1} (Figure 3c, bottom). There is hence no obvious correlation ~~of~~ between the red-shift~~ed~~ and strength of the amide I absorption band with the observation of a large VCD signal. It is possible, however, that subtle differences in the supramolecular arrangement of aggregates with different strand lengths[31] may cause strong variations in VCD intensity. This explanation does, of course, not pertain to the isotope series, since the UV/vis and ECD spectra of the ^{13}C-labeled compounds **3*a**–**c** clearly show that their internal arrangement was identical.

2D-IR Spectroscopy. Two-dimensional infrared (2D-IR) spectroscopy correlates different vibrational bands by first exciting and then probing multiple infrared transitions.[37] Cross peaks between vibrations arise from anharmonic coupling between vibrations. In our systems, they will indicate whether labeled and unlabeled carbonyl groups give rise to mixed or separate exciton transitions, or show a mixing of amide I and perylene bisimide vibrations. The diagonal peaks, on the other hand, are much more sensitive to redistribution of oscillator strength than the linear FTIR spectra, as they scale to the fourth power of the transition dipole moments. Their shape can also reveal the broadening mechanism underlying the band shape. We therefore screened the 2D-IR spectra of nanofibril solutions of the isotope-labeled compounds **3*a–c** and the unlabeled compounds **3** and **4** for conspicuous similarities or irregularities (Figure 4, Supplementary Figure S5). All 2D-IR spectra had in common the signals of the perylene bisimide chromophores (linked by the red squares in Figure 4a), which allowed us to normalize the plots for the diagonal peak near $(\omega_{pump}, \omega_{probe})/hc = 1700\ cm^{-1}$.

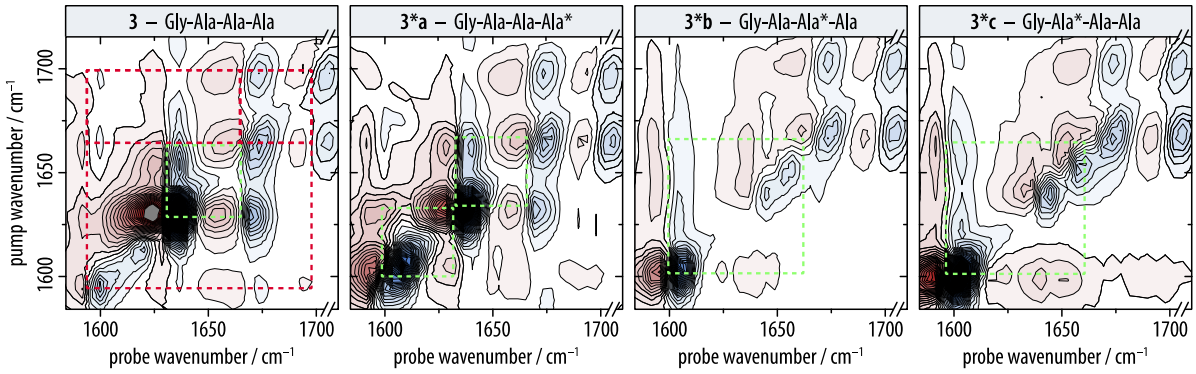

Figure 4. 2D-IR spectra of the unlabeled compound **3** as compared to the ^{13}C-labeled derivatives **3*a–c** (TCE, $1 \cdot 10^{-3}$ mol/L, perpendicular polarization of pump and probe pulses). The asterisk marks the position of the ^{13}C-labeled carbonyl carbon in the peptide sequence. The excited state absorption resulting in positive signals is shown in red; the combination of ground state bleaching and stimulated emission leading to negative signals is marked in blue. The dashed red squares in **3** highlight the coupling patterns of the three perylene bisimide vibrations in the amide I region, and the dashed green squares in **3*a–c** and **3** highlight the cross-couplings as discussed in the main text.

The amide I band of the unlabeled sample **3** at 1630 cm^{-1} gave rise to an intense diagonal peak with a vertical line separating the excited state absorption (red, positive) from ground state bleach and stimulated emission (blue, negative) in the 2D contour plots. The band is thus completely homogeneously broadened, and its anharmonicity is smaller than the bandwidth,

consistent with a delocalized excitonic system.[38] By contrast, the diagonal peaks of the perylene bisimide C=O stretch modes of **3** at 1665 and 1700 cm^{-1} were tilted towards the diagonal due to inhomogeneous broadening, which suggested that they were not part of an exciton system. However, the cross peaks at $(\omega_{pump}, \omega_{probe})/hc$ = (1630, 1665) cm^{-1} and (1655, 1630) cm^{-1} were a sign of considerable coupling of the amide I mode with the perylene bisimide C=O stretch vibration of b_{3u}-symmetry. A similar set of cross peaks between perylene bisimide and the strong regular (^{12}C) amide I band of the peptide was also observed in the case of isotope-labeled sample **3*a**. In contrast, the other two isotope labled compounds **3*b** and **3*c** exhibited much weaker regular amide I signals, reflecting the splitting of the corresponding absorption bands in the FTIR spectra. Thus the 2D-IR spectra highlight the strong disruption of the amide I exciton band when the ^{13}C isotope labels are introduced in the second or third carbonyl of the peptides strands, while the effect is much weaker when the outermost carbonyls are labeled. This trend correlates well with the observation of strongly enhanced VCD in the case of **3** and **3*a** as opposed to **3*b** and **3*c**. However, control measurements of **4**, a compound that showed very weak circular dichroism signals, yielded a 2D-IR spectrum with an even stronger excitonic amide I signal and a similar cross peak pattern as for **3** and **3*a (**Supplementary Figure S5). We did thus not observe any features in the 2D-IR spectra that are unique to compounds with an enhanced VCD and would allow to distinguish compounds with a comparably strong excitonic amide I signal with or without a strong Cotton effect.

The 2D-IR spectra nevertheless showed significant intensity borrowing by the isotope labeled amide I bands of **3*a**–**c** from the regular amide I transition. The corresponding isotope-labeled diagonal peaks even dominated the 2D-IR spectra of **3*b** and **3*c.** Furthermore, like the 'native' amide I band of the unlabeled sample **3**, the diagonal peaks of **3*b** and **3*c** near 1600 cm^{-1} had almost vertical line shapes with small anharmonicities, indicating that the corresponding exciton transitions were also delocalized. This was, however, not sufficient for generating a significant isotope-shifted VCD signal.

Computational Modelling. We complemented our experimental investigations with simulations using a transition dipole coupling model[39] in combination with a nearest neighbor coupling map.[40,41] Compared to more sophisticated computations based on density functional theory,[23,24] this approach makes it possible to efficiently explore a large number of structural parameters and size-effects. Transition dipole coupling simulations have recently been used to establish signal-structure relationships in fibrillar nanostructures from β-sheet-forming protein residues[25,26] or helical polymers of isocyanopeptides.[9] Our set of helical or twisted β-sheet helices with a well-defined morphology and a strong isotope effect may be regarded as a very suitable test case for the predictive power of such calculations. For the simulation of our system, the information from X-ray data and AFM imaging served as a guideline (Figure 5).[30] The simulations were performed on β-sheet structures with a width of *k* amino acid residues and a length of *m* β-strands, in order to elucidate the influence of peptide dihedral angles, helix handedness, β-sheet length, as well as the possible role of intersheet coupling.

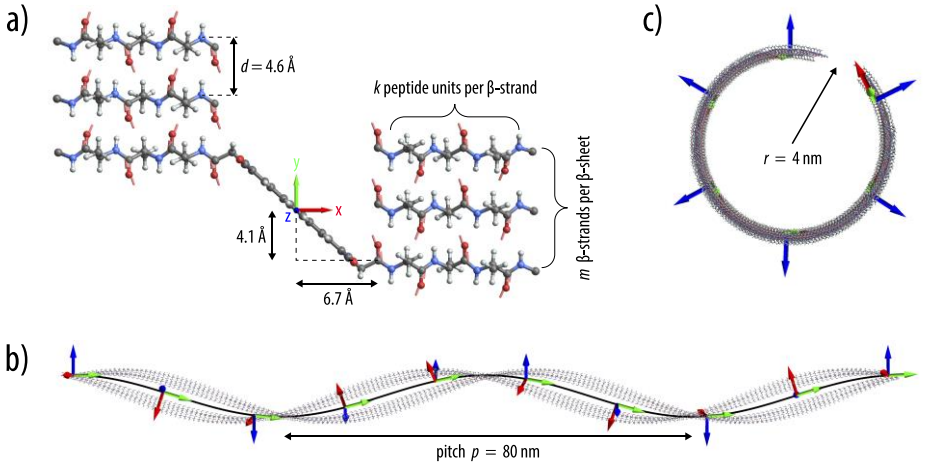

Figure 5. Schematic illustration of the structural parameters used in the simulations. *a)* Each of the two entwined β-sheet helices consisted of *m* β-strands comprising $k = 4$ amino acid residues. Localized amide I transition dipoles (0.25 Debye, orange arrows) where assumed to lie in the peptide planes at 0.83 Å from the carbon atom along the C=O bond and with a 20° angle between the dipole and the C=O direction.[42] The entwined β-sheet structure was constructed from building blocks that consisted of one β-strand for each sheet with the innermost C=O groups oriented in opposite directions parallel to the long axis of the β-sheets. The line joining the first and third carbonyl carbon of each β-strand was parallel to the *x* axis of a building block (the long axis of the β-strand), and the *xy* plane of a building block conincided with the peptide planes of the innermost peptide units. The innermost carbonyl carbons of the two β-strands were displaced by $\Delta x = \pm 6.7$ Å and $\Delta y = \pm 4.1$ Å from the local origin at the center of the π–π stacked perylene bisimides. *b)* Side view and *c)* view along the long axis of the full structure: local origins of the *m* building blocks were distributed along a helical coil with radius $r = 40$ Å and pitch $p = 800$ Å, and placed at a distance $d = 4.6$ Å. Each building block was rotated such that its local *z* axis was radial and its *y* axis pointed along the helix towards the center of the next unit. See the supporting information for further details.

Effect of Dihedral Angles. The dihedral angles between adjacent amino acids in parallel β-sheets may be chosen from a relatively wide area in the Ramachandran plot. For our simulations, we compared the spectra of single oligopeptide β-strands ($m = 1$) and β-sheets ($m = 21$) using average dihedral angles (φ, ψ) = (–120°, 115°), (–130°, 130°) and (-140°, 145°), chosen from Gaussian distributions with FWHM of 5° to account for structural heterogeneity. The first two pairs of angles are the 'canonical' angles found in proteins[43] while the latter is an average reported for helical poly(isocyanide)s comprising β-sheet-forming side groups[10] and are in good agreement with dihedral angles found in our previous MD simulations.[30] Local amide I frequencies were taken from a Gaussian distribution centered at 1650 cm^{-1} with width of 20 cm^{-1}, and an isotope shift of –40 cm^{-1} was used for ^{13}C-labeled residues.

Single β-strands ($k = 4$, $m = 1$) generated with the three choices of dihedral angles gave rise to very different VCD amplitudes (Figure 6a, bottom, thin lines). These differences became less pronounced for the double β-sheet structures ($k = 4$, $m = 21$), for which the signals were approximately 2–10 times larger and shifted to lower frequencies as compared to the single β-strands. By contrast, the simulated IR spectra were much less sensitive to the dihedral angles (Figure 6a, top). A strong excitonic shift and band narrowing was observed in all cases, while a high frequency shoulder for larger dihedral angles appeared to coincide with more intense VCD couplets. While these results led us to adopt dihedral angles (φ, ψ) = (–140°, 145°) for most of the subsequent simulations, the sensitivity to small parameter variations should probably be regarded as a caveat against over-interpreting the simulations, given the approximations of the chosen model.

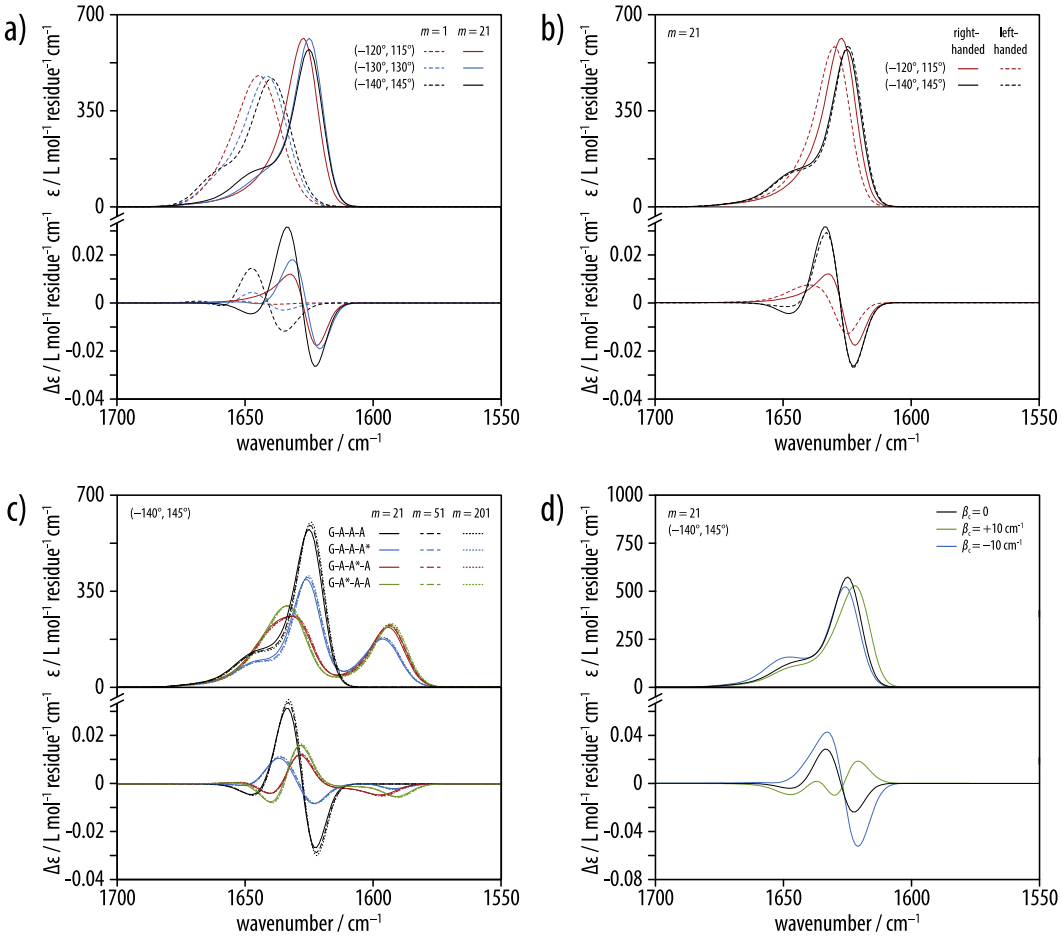

Figure 6. *a)* Simulated IR (top) and VCD spectra (bottom) for different choices of dihedral angles (φ, ψ) = (–120°, 115°, red), (–130°, 130°, blue), and (–140°, 145°, black). Dashed lines represent single β-strands (m = 1) and bold lines represent sections of right-handed parallel β-sheet helices (m = 21) with a pitch of 80 nm and a radius of 4 nm (Figure 5). *b)* Comparison of β-sheet helices (m = 21) with opposite handedness (solid lines: right-handed, dashed lines: left-handed) for different choices of dihedral angles (φ, ψ) = (–120°, 115°, red) and (–140°, 145°, black). *c)* Effect of isotope labelling and β-sheet length, without isotope label (black) and ^{13}C-labeled L-alanines at the strand position marked with an asterisk (A*, G = glycine; blue, red, and green curves). Solid lines: m = 21, dashed lines: m = 51, dotted lines m = 201. Right-handed helices with (φ, ψ) = (–140°, 145°) for all spectra in *c)*. *d)* Effect of additional coupling across the perylene bisimide core: transition dipole coupling only (black), additional coupling β_C = +10 cm^{-1} (green) and β_C = –10 cm^{-1} (blue) for (φ, ψ) = (–140°, 145°). Right-handed helices for all spectra in *d)*. k = 4 for all spectra in *a)–d)*.

Helix-Handedness. In simulations of β-sheets ((φ, ψ) = (–140°, 145°), k = 4, m = 21) with opposite helix handedness, both IR and VCD spectra were almost indistinguishable. Remarkably, the VCD couplet for structures of opposite handedness thus exhibited the same sign (Figure 6b, bottom). For a different choice of dihedral angles (φ, ψ) = (–120°, 115°) (thin lines in Figure 6b), the spectra can be substantially different depending on the handedness, but we never observed opposite signs. One must conclude that the sign of the VCD couplet predicted by the transition dipole coupling model can not differentiate parallel β-sheets with opposite helicity if these are formed from the same oligopeptides. Because of the given molecular chirality of the β-strands formed from L-alanine residues (that are reflected in the

preferred dihedral angles φ and ψ), aggregates with opposite handedness are diastereomers. Remarkably, however, the local chirality becomes the factor determining the VCD sign. In our simulations, only truly enantiomeric aggregates comprising a single carbonyl group per strand ($k = 1$, $m = 21$) gave VCD signals that were mirror images of one another (Supplementary Figure S6). This is an aspect that should be taken into account when the VCD sign is used to probe the handedness of aggregates, as in the recent example by Aparicio *et al.*.[11] Similar to our results, it has been reported previously that DFT-calculations predicted VCD couplets of oposite sign for helical polymers of isocyanopeptides of the same handedness.[10] On the other hand, the correspondence of left-handed fibrils to negative VCD couplets has been well established for amyloid-type aggregates (while positive couplets have been observed but could not be unambiguously assigned to right-handed aggregates),[2] where, contrary to our system, β-sheet stacking is believed to be the origin of enhanced VCD.[24,25]

β-Sheet Length and Isotope-Labeling. Increasing the number of β-strands beyond $m = 21$ did not significantly change the simulated absorption, neither for the unlabeled nor for the ^{13}C-labeled β-sheets (Figure 6c, top). The frequency shift and change in extinction coefficient of amide I and ^{13}C isotope peaks were in qualitative agreement with our experimental observations. Moreover, the simulated spectrum of **3*b** also exhibited a splitting of the main amide I band, although the even larger split for **3*c** was not properly reproduced. Similar to the experiment, the relative strength of the isotope-shifed bands of 40% was significantly larger than the 25 mol% of ^{13}C-labeled carbonyls would imply. This intensity borrowing of the isotope-shifted amide I band is frequently encountered in exciton systems with almost parallel local dipoles (for instance, in labeled α-helices[44] and β-sheets[13,24]) that lead to a redistribution of oscillator strength in favor of the lowest energy exciton transition. The simulations thus qualitatively accounted for prominent features in the experimental IR and 2D-IR spectra. Likewise, sign and shape of the VCD signals for **3** and **3*a** were qualitatively reproduced, but the isotope effect (no VCD for **3*b** and **3*c)** was not. Most importantly, independent of the choice of dihedral angles, the simulated IR and VCD intensities converged already for a small number of β-strands ($m < 50$, Figure 6c, bottom) representing significantly less than a full helix

turn (m = 180). Moreover, the simulated $\Delta\varepsilon/\varepsilon$ ratio of $5 \cdot 10^{-5}$ was two orders of magnitude smaller than the experimental value. The transition dipole coupling model, hence, does not account for (very) long range order, and the moderate VCD enhancement observed in small aggregates compared to the individual β-strands described above can not simply be extrapolated to explain the giant VCD observed in larger systems.

Intersheet Coupling: Our simulations considering only one of the two connected β-sheets yielded essentially the same results as those for the full structures for dihedral angles (φ, ψ) = (–140°, 145°), reflecting the weak transition dipole coupling between carbonyls across the perylene bisimide core. Interestingly, however, significant VCD was only observed for the double sheet structure for dihedral angles (φ, ψ) = (–120°, 115°) (Supplementary Figure S7). An additional perylene-mediated 'through-bond' contribution to the coupling between the two β-sheet segments could also not be excluded *per se* because the 2D-IR spectra had indicated some coupling between the C=O stretch modes (b_{3u}) of the perylene bisimide and the oligopeptide side chains (although, at the same time, the perylene bisimide carbonyls did not appear to participate strongly in the exciton system). For this reason, we explored the effect of an *ad hoc* coupling constant of $\beta_c = \pm$ 10 cm^{-1} between the carbonyls of the glycine residues at the *N*-termini of each of the two β-strands (Figure 6d). The additional negative coupling enhanced the VCD signal by more than a factor of two, while a positive coupling constant reversed the sign of the simulated VCD couplet. However, the sign of the VCD couplet remained the same for aggregates with opposite handedness as already observed before (Supplementary Figure S8a–b), thus bearing no direct connection to the overall structure of the molecules. Spectra converged for approximately m = 51 β-strands and the VCD intensities with and without isotope labels were similar, as for the case $\beta_c = 0$ (Supplementary Figure S8c–d).

Conclusions

In summary, we observed a negative, giant VCD couplet for self-assembled nanofibrils from oligopeptide-substituted perylene bisimides that were independently shown to comprise single tapes without β-sheet stacking, challenging the current assumption that the latter is the main origin of enhanced VCD in amyloid-like assemblies. At the same time, we provided the first example of oligopeptide aggregates in which an enhanced negative ('normal') VCD couplet for the amide I absorption can be explicitly assigned to right-handed helical aggregates, raising concerns about the unique assignment of supramolecular handedness based on VCD spectroscopy. The giant VCD signal almost completely disappeared upon ^{13}C isotope labeling, imposing strict constraints on the possible origins of the large Cotton effect. 2D-IR spectroscopy confirmed that a strong disruption of the exciton system upon isotope labeling was associated with the vanishing of the VCD signal, but could not reveal distinct coupling features for systems with and without enhanced VCD. Thus 2D-IR spectroscopy only provides limited additional information when applied to extended fibrilar structures. Simulations based on a transition dipole coupling model, which had previously been claimed to account for the strong vibrational optical activity of amyloids,[25] qualitatively reproduced the IR spectra of both non-labeled and ^{13}C-labeled β-sheets but failed to account for the observed giant VCD or the strong isotope effect. It is thus generally questionable if a local coupling approach can adequately describe the chiral spectra of systems already of the size of the investigated nanofibrils. This may even be difficult when more sophisticated first principle methods are employed. For instance, Welch *et al.* reported that VCD enhancement due to β-sheet stacking saturated far below the experimental value and was strong only for flat β-sheets.[23,24] Treated on the DFT level individual β-sheets, which were then arranged in stacks coupled by transition dipole interaction

coupling to produce stronger VCD signals. A similar approach could be taken for the extended helical structures presented here, by coupling the excitonic dipoles of smaller sections of the parallel β-sheets. Since isotope labelling disrupts the excitonic system, smaller excitonic transition dipoles could then lead to strongly diminished VCD signals of the isotope-labelled structures. Given the significant influence of intersheet coupling on the simulated spectra,

however, a proper modelling of the perylene bisimide backbone may nevertheless be required. Our results illustrate that with our present understanding we cannot yet reliably use these remarkable signals for the structural characterization of new compounds. The well-defined structure of the nanofibrils and the spectroscopic evidence reported in this paper will thus be a benchmark test for any model designed to describe strong VCD in peptide aggregates and nanostructures.

Associated Content

Supporting Information. Supplementary Schemes S1–S2, Supplementary Figures S1–S10, and details about UV/vis, ECD, IR, VCD, and 2D-IR spectroscopy as well as about AFM imaging. Furthermore, the supporting information contains details on the synthesis, NMR, and mass spectra of compounds **3*a**–**c**, and all intermediates, as well as computational details including the executable source code. This material is available free of charge *via* the Internet at http://pubs.acs.org.

Author Information

Corresponding Author

jan.helbing@chem.uzh.ch

Notes

The authors declare no competing financial interest.

Acknowledgments

The authors would like to thank Prof. Clémence Corminboeuf (*Ecole Polytechnique Fédérale de Lausanne, Switzerland*) and Stephan N. Steinmann for providing the MD simulations. Furthermore, funding from the *Swiss National Science Foundation* (SNF Grant 200020_144417 to H.F. and 200020_143487 to J.H.) is gratefully acknowledged.

References

(1) Ma, S.; Cao, X.; Mak, M.; Sadik, A.; Walkner, C.; Freedman, T. B.; Lednev, I. K.; Dukor, R. K.; Nafie, L. A. *J. Am. Chem. Soc.* **2007**, *129*, 12364.

(2) Kurouski, D.; Dukor, Rina K.; Lu, X.; Nafie, Laurence A.; Lednev, Igor K. *Biophys. J.* **2012**, *103*, 522.

(3) Dzwolak, W.; Kalinowski, J.; Johannessen, C.; Babenko, V.; Zhang, G.; Keiderling, T. A. *J. Phys. Chem. B* **2012**, *116*, 11863.

(4) Kurouski, D.; Lu, X.; Popova, L.; Wan, W.; Shanmugasundaram, M.; Stubbs, G.; Dukor, R. K.; Lednev, I. K.; Nafie, L. A. *J. Am. Chem. Soc.* **2014**.

(5) Measey, T. J.; Smith, K. B.; Decatur, S. M.; Zhao, L.; Yang, G.; Schweitzer-Stenner, R. *J. Am. Chem. Soc.* **2009**, *131*, 18218.

(6) Shanmugam, G.; Polavarapu, P. L. *J. Struct. Biol.* **2011**, *176*, 212.

(7) Nieto-Ortega, B.; Nebot, V. J.; Miravet, J. F.; Escuder, B.; Navarrete, J. T. L.; Casado, J.; Ramírez, F. J. *J. Phys. Chem. Lett.* **2012**, *3*, 2120.

(8) Shanmugam, G.; Polavarapu, P. L. *Biochim. Biophys. Acta* **2013**, *1834*, 308.

(9) Schwartz, E.; Domingos, S. r. R.; Vdovin, A.; Koepf, M.; Buma, W. J.; Cornelissen, J. J. L. M.; Rowan, A. E.; Nolte, R. J. M.; Woutersen, S. *Macromolecules* **2010**, *43*, 7931.

(10) Schwartz, E.; Liégeois, V.; Koepf, M.; Bodis, P.; Cornelissen, J. J. L. M.; Brocorens, P.; Beljonne, D.; Nolte, R. J. M.; Rowan, A. E.; Woutersen, S.; Champagne, B. *Chem. Eur. J.* **2013**, *19*, 13168.

(11) Aparicio, F.; Nieto-Ortega, B.; Nájera, F.; Ramírez, F. J.; López Navarrete, J. T.; Casado, J.; Sánchez, L. *Angew. Chem. Int. Ed.* **2014**, *53*, 1373.

(12) Brauner, J. W.; Dugan, C.; Mendelsohn, R. *J. Am. Chem. Soc.* **2000**, *122*, 677.

(13) Kubelka, J.; Keiderling, T. A. *J. Am. Chem. Soc.* **2001**, *123*, 6142.

(14) Decatur, S. M. *Acc. Chem. Res.* **2006**, *39*, 169.

(15) Ganim, Z.; Chung, H. S.; Smith, A. W.; DeFlores, L. P.; Jones, K. C.; Tokmakoff, A. *Acc. Chem. Res.* **2008**, *41*, 432.

(16) Wang, J.; Chen, J.; Hochstrasser, R. M. *J. Phys. Chem. B* **2006**, *110*, 7545.

(17) Backus, E. H. G.; Bloem, R.; Donaldson, P. M.; Ihalainen, J. A.; Pfister, R.; Paoli, B.; Caflisch, A.; Hamm, P. *J. Phys. Chem. B* **2010**, *114*, 3735.

(18) Falvo, C.; Zhuang, W.; Kim, Y. S.; Axelsen, P. H.; Hochstrasser, R. M.; Mukamel, S. *J. Phys. Chem. B* **2012**, *116*, 3322.

(19) Wang, L.; Middleton, C. T.; Singh, S.; Reddy, A. S.; Woys, A. M.; Strasfeld, D. B.; Marek, P.; Raleigh, D. P.; de Pablo, J. J.; Zanni, M. T.; Skinner, J. L. *J. Am. Chem. Soc.* **2011**, *133*, 16062.

(20) Woys, A. M.; Almeida, A. M.; Wang, L.; Chiu, C.-C.; McGovern, M.; de Pablo, J. J.; Skinner, J. L.; Gellman, S. H.; Zanni, M. T. *J. Am. Chem. Soc.* **2012**, *134*, 19118.

(21) Lee, C.; Cho, M. *J. Phys. Chem. B* **2004**, *108*, 20397.

(22) Kubelka, J.; Keiderling, T. A. *J. Am. Chem. Soc.* **2001**, *123*, 12048.

(23) Welch, W. R. W.; Kubelka, J.; Keiderling, T. A. *J. Phys. Chem. B* **2013**, *117*, 10343.

(24) Welch, W. R. W.; Keiderling, T. A.; Kubelka, J. *J. Phys. Chem. B* **2013**, *117*, 10359.

(25) Measey, T. J.; Schweitzer-Stenner, R. *J. Am. Chem. Soc.* **2011**, *133*, 1066.

(26) Schweitzer-Stenner, R. *J. Phys. Chem. B* **2012**, *116*, 4141.

(27) Aggeli, A.; Nyrkova, I. A.; Bell, M.; Harding, R.; Carrick, L.; McLeish, T. C. B.; Semenov, A. N.; Boden, N. *Proc. Natl. Acad. Sci. U.S.A.* **2001**, *98*, 11857.

(28) Frauenrath, H.; Jahnke, E. *Chem. Eur. J.* **2008**, *14*, 2942.

(29) Tian, L. F.; Szilluweit, R.; Marty, R.; Bertschi, L.; Zerson, M.; Spitzner, E. C.; Magerle, R.; Frauenrath, H. *Chem. Sci.* **2012**, *3*, 1512.

(30) Marty, R.; Szilluweit, R.; Sánchez-Ferrer, A.; Bolisetty, S.; Adamcik, J.; Mezzenga, R.; Spitzner, E.-C.; Feifer, M.; Steinmann, S. N.; Corminboeuf, C.; Frauenrath, H. *ACS Nano* **2013**, *7*, 8498.

(31) Marty, R.; Nigon, R.; Leite, D.; Frauenrath, H. *J. Am. Chem. Soc.* **2014**, *136*, 3919.

(32) Würthner, F.; Sautter, A.; Schmid, D.; Weber, P. J. A. *Chem. Eur. J.* **2001**, *7*, 894.

(33) Thalacker, C.; Würthner, F. *Adv. Funct. Mater.* **2002**, *12*, 209.

(34) Chen, Z.; Stepanenko, V.; Dehm, V.; Prins, P.; Siebbeles, L. D. A.; Seibt, J.; Marquetand, P.; Engel, V.; Würthner, F. *Chem. Eur. J.* **2007**, *13*, 436.

(35) Dehm, V.; Chen, Z.; Baumeister, U.; Prins, P.; Siebbeles, L. D. A.; Wurthner, F. *Org. Lett.* **2007**, *9*, 1085.

(36) Akers, K.; Aroca, R.; Hor, A. M.; Loufty, R. O. *Spectrochim. Acta* **1988**, *44A*, 1129.

(37) Hamm, P.; Zanni, M. *Concepts and Methods of 2D Infrared Spectroscopy*; Cambridge University Press: Cambridge, UK, 2011.

(38) Edler, J.; Hamm, P. *J. Chem. Phys.* **2002**, *117*, 2415.

(39) Gulotta, M.; Goss, D. J.; Diem, M. *Biopolymers* **1989**, *28*, 2047.

(40) Hamm, P.; Woutersen, S. *Bull. Chem. Soc. Jpn.* **2002**, *75*, 985.

(41) la Cour Jansen, T.; Dijkstra, A. G.; Watson, T. M.; Hirst, J. D.; Knoester, J. *J. Chem. Phys.* **2006**, *125*.

(42) Torii, H.; Tasumi, M. *J. Chem. Phys.* **1992**, *96*, 3379.

(43) Voet, D.; Voet, J. G. *Biochemistry*, 2nd ed. John Wiley & Sons Inc.: New York, 1995.

(44) Silva, R. A. G. D.; Kubelka, J.; Bour, P.; Decatur, S. M.; Keiderling, T. A. *Proc. Natl. Acad. Sci. U.S.A.* **2000**, *97*, 8318.